A Low-Cost Wideband Reflectarray Antenna Based on Nonradiative Dielectric Waveguide

Wen Wu, Kai-Da Xu, *IEEE Senior Member*, Qiang Chen, *IEEE Senior Member*, Toru Tanaka, Masaki Kozai, and Hiroya Minami

***Abstract*—A wideband reflectarray antenna (RA) with improved efficiency is proposed based on nonradiative dielectric (NRD) waveguide unit cells. The inherent non-resonant nature of the waveguide is utilized to achieve wideband performance. In contrast to conventional rectangular waveguide (RWG) based RA, the proposed design simplifies the unit cell structure by eliminating a pair of conductor walls and the metal ground used for reflecting the incident electromagnetic wave. Additionally, the proposed design achieves a compact unit cell size of 0.43λ×0.44λ, where λ represents the free-space wavelength at the center frequency (10 GHz). The single-layer dielectric is employed for the RA design instead of previously reported multilayer or stacked layers to achieve the comparable performance. The prototype consists of 16 ×16 unit cells, with the dielectric components fabricated by 3D printing technology. The measurements show that the 1-dB and 3-dB gain bandwidths of 18% and 27% are realized, respectively, with a peak aperture efficiency of 45%. Both of the simulations and measurements validate that the proposed design enables wideband and improved efficiency using a low-cost compact structure.**

***Index Terms*—Nonradiative dielectric waveguide (NRD), reflectarray antenna, wideband, cutoff frequency.**

I. Introduction

REFLECTARRAY antennas (RAs) are a crucial technology in B5G/6G communication systems that provide reliable high-speed communication channels for data centers and other infrastructure [1][2]. As network deployments continue to grow exponentially, the need for wideband, high-gain and low-cost RAs is becoming increasingly urgent [3]. A number of studies have examined wideband RAs using frequency-independent resonant elements to achieve wideband radiative performance through rotating or complementary structures fabricated by printed circuit board (PCB) technology [4]-[9]. However, multi-dimensional PCB structures are expensive, especially for larger apertures [10], and the metal loss cannot be ignored in millimeter-wave applications. Alternatively, dielectric-based RAs offer a cost-efficient design solution that can be utilized up to terahertz frequencies.

Typical dielectric RA designs involve printing or placing dielectric slabs on a conductor ground using 3D printing or substrate processing technology. In [11] and [12], the dielectric slabs are fabricated with varying heights and serve as grooved Fresnel zone plate (FZP) reflectors, achieving a wide 1-dB gain bandwidth of over 18% but at the expense of worsened aperture efficiency due to the adjacent blocking effect in the non-planar structure. In contrast, the work in [13] presents a planar structure using perforated dielectric slabs with an aperture efficiency of approximately 40%, yet the gain bandwidth is limited to only 7% due to the nonlinear relationship between effective permittivity and reflection phase in the perforated elements. Dielectric resonator antennas (DRA) are also employed as discrete unit cells for planar dielectric RA designs [14][15] and the tuning of reflection phases is achieved by adjusting the width or radius of the dielectric slab. However, the inherent resonant nature of DRA elements makes it difficult to achieve an operating bandwidth of exceeding 10%. Enhancing both bandwidth and efficiency remains a challenge for dielectric RAs, and currently the available method is often using complex configurations such as multilayer [16] or stacked layers [17].

The non-radiative dielectric (NRD) waveguide [18][19] is a compact and low-loss waveguide that can serve as a potential unit cell in planar RAs. It allows for direct reception of the incident wave without adjacent blockage effect and exhibits a non-resonant nature, which is suitable for achieving the performance of wideband and high efficiency simultaneously.

In this letter, for the first time, we utilize a single-layer dielectric within a waveguide structure to achieve enhanced bandwidth and efficiency simultaneously. The periodicity of the proposed unit cell is 0.43λ in the longitudinal direction and 0.44λ in the lateral direction, with λ representing the free-space wavelength at the center frequency (10 GHz) of the RA. It is significantly smaller than that required in rectangular waveguide (RWG) based RAs [20]-[22], where the periodicity falls within the range of 0.6 to 0.7 times of the free-space wavelength at the center frequency. Moreover, the proposed design simplifies the structure by removing a pair of conductor walls and the metal ground in each RWG unit cell. Simulations and measurements of the proposed design show that its bandwidth and aperture efficiency is comparable to those of multilayer dielectric RAs.

II. Unit Cell Design

The RA using a space-fed configuration can eliminate the need of complex feed network, which enables convenient utilization of NRD waveguide as the unit cell of large-scale

This work was supported in part by the Program on Open Innovation Platform with Enterprises, Research Institute and Academia, Japan Science and Technology Agency (JST, OPERA, JPMJOP1852). (Corresponding author: Kai-Da Xu.)

Wen Wu, Kai-Da Xu and Qiang Chen are with the Department of Communications Engineering, Tohoku University, Sendai 980-8579, Japan. (e-mail: kaidaxu@ieee.org)

T. Tanaka, M. Kozai and H. Minami are with the NTT Space Environment and Energy Laboratories, NTT Corporation, Tokyo 180-8585, Japan.

array antenna, resulting in a more streamlined and concise structure. The configuration of the proposed NRD waveguide as the RA unit cell is depicted in Fig. 1. The electromagnetic (EM) wave is confined within a dielectric slab with cross-section dimensions of $a \times b$ and height of h_d, due to the difference in dielectric constants between the dielectric and the surrounding air. This feature of NRD waveguide eliminates strong surface currents that can occur on the metallic walls of RWG. The dimensions of the dielectric slab within the unit cell are set to 13 mm and 10 mm for a and b, respectively. The chosen dielectric material is polylactic acid (PLA), known for its cost-effective application as a 3D printing filament, featuring a typical permittivity of 2.7 and a loss tangent of 0.01. The conductor wall has a height of 30 mm (h = 30 mm) and a thickness of 0.3 mm. The dielectric slab maintains uniformity and continuity along the direction of electromagnetic wave propagation, defining a single-layer configuration, which is consistent with the descriptions in [11]-[15].

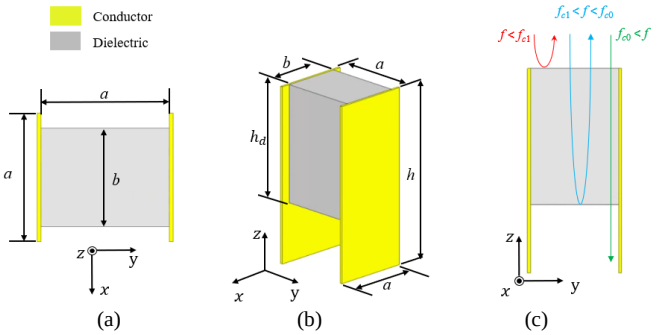

Fig. 1. The proposed NRD waveguide. (a) Top view, (b) perspective view, and (c) working mechanism as the RA unit cell.

For a parallel-plate waveguide without embedding a dielectric slab, the lowest frequency that EM waves can propagate, i.e., the cutoff frequency f_{c0} is determined by the distance a between the two parallel metal plates, where the value of a should be chosen as around half of the free-space wavelength λ_{c0} at frequency f_{c0}. However, when a dielectric slab is embedded into the waveguide, the effective width of the waveguide for the EM wave is increased, leading to a decrease of the cutoff frequency. As the frequency falls below f_{c1} (corresponding to the free space λ_{c1}), the incident EM wave will be blocked from propagating, even within the dielectric slab. The frequency f_{c1} acts as the lower cutoff frequency, which is associated with the dominant propagation mode, known as the longitudinal section magnetic mode (LSM_{11}) in NRD waveguide.

When utilized as the unit cell of the proposed reflectarray, the NRD waveguide is terminated by an open end, which causes the incident EM wave to reflect and creates two cutoff frequencies: f_{c1} and f_{c0}, as illustrated in Fig. 1(c). The EM waves below f_{c1} will be reflected around the surface of the NRD waveguide, while those with frequencies above f_{c0} will propagate through the dielectric and radiate from the other end of the waveguide. Therefore, the effective bandwidth of the unit cell is determined by the difference between f_{c0} and f_{c1}.

It is important to note that the bandwidth is influenced by the physical dimensions of the waveguide and the permittivity of the dielectric slab. When the physical dimensions of the unit cell remain constant, a higher dielectric permittivity will lead to a decrease in f_{c1}, while f_{c0} remains unchanged, resulting in an extended bandwidth. As mentioned in [18], the bandwidth of an NRD waveguide is determined by a bandwidth factor (BW_{factor}) which is calculated based on the permittivity and the width-to-length ratio of its cross-section. The calculation of BW_{factor} can be performed using the following formula:

$$BW_{factor} = \sqrt{\varepsilon_r - 1} \times b / a \quad (1)$$

where ε_r is the relative permittivity and b/a is the width-to-length ratio of the dielectric slab cross-section. For the permittivity of 2.7, an optimal BW_{factor} range of 1.0 to 2.0 is found to achieve the maximum bandwidth.

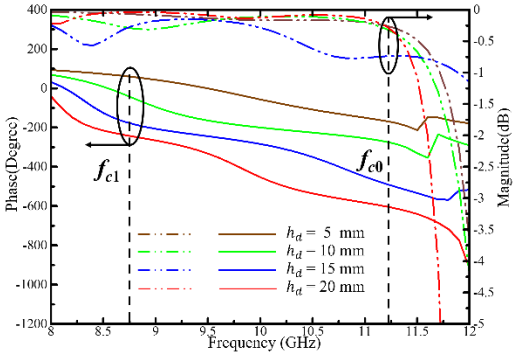

Fig. 2. Simulated reflection amplitude and phase versus frequency for the NRD waveguide unit cell with different values of h_d, where a =13 mm, b =10 mm, h = 30 mm.

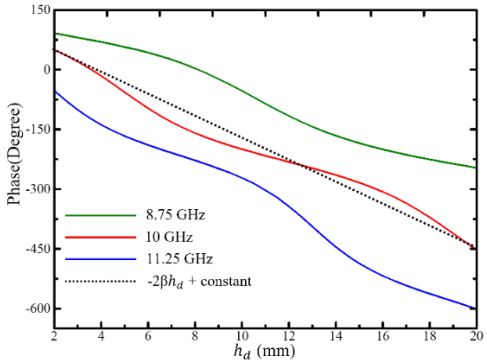

Fig. 3. Simulated reflection phase versus h_d at different frequencies.

The reflection phase of the NRD waveguide within the frequency range between f_{c1} and f_{c0} can be controlled by adjusting the height h_d of the dielectric slab, which determines the propagation length in the waveguide, as shown in Fig. 1(c). Full-wave EM simulations are conducted using Ansys HFSS to evaluate the reflection performance of the unit cell and determine the cutoff frequencies. The simulations employ Floquet port excitation with periodic boundary condition. Fig. 2 illustrates the results obtained for the varied height of the dielectric slab (h_d).

The selection of f_{c0} is based on the frequency point above which the amplitude of the reflection coefficient S_{11} rapidly decreases. On the other hand, f_{c1} should be selected to ensure that the phase shift range provided by different lengths of dielectric slab is sufficient for phase tuning in the reflectarray design. Following the above guideline, the highest operating frequency f_{c0} is selected as 11.25 GHz, at which the minimum

reflection coefficient magnitude reaches -0.7 dB. The cross-sectional width (a=13 mm) of the NRD waveguide is close to and smaller than half of its corresponding free space wavelength (i.e., $0.5\lambda_{c0}$ =13.33 mm). This value is significantly smaller compared to the dimension of conventional RWGs, where a should be larger than the wavelength of the cutoff frequency (lowest operating frequency). Furthermore, f_{c1} is determined to be 8.75 GHz, which enables a reflection phase range of at least 300° to be achieved by adjusting the height of the dielectric slab h_d between 5 mm and 20 mm.

Accordingly, the operating frequency range of the proposed unit cell spans from 8.75 GHz to 11.25 GHz. At the center frequency of 10 GHz, the reflection phase provided by the NRD waveguide is evaluated as a linear function of h_d, as depicted by the dashed line in Fig. 3, in which the slope of the phase with respect to h_d is 2β, and β represents the propagation constant of NRD waveguide at 10 GHz. As a result, by adjusting the value of h_d, the reflection phase of the unit cell can be precisely tuned for reflectarray design. The average magnitude of the reflection coefficient against the varied h_d values is -0.28 dB, and the primary factor influencing the power loss in the reflection wave is associated with the dielectric material, rather than ohmic loss.

III. Reflectarray Design, Fabrication and Results

The RA based on the proposed NRD waveguide unit cell is designed in this section to verify its performance. The unit cell has a physical dimension of 13 mm × 13.3 mm (including the conductor wall thickness of 0.3 mm). Meanwhile, the prototype of the RA comprises a configuration of 16 × 16 unit cells with an aperture size of 6.9λ × 7.1λ, where λ denotes the free-space wavelength at the center frequency of 10 GHz. The feed is selected as a 15 dBi standard gain horn antenna (A-INFO LB-90-15) with its axial direction in the *yoz* plane and offset at a 20° angle towards the broadside direction to minimize the aperture blockage effect. The focus-to-diameter ratio (F/D) is set as 1.0 to ensure that the illumination tapper at the edge of the aperture is below -10 dB. The calculated spillover efficiency and illumination efficiency are 90% and 83%, respectively. The collimated beam is designed to have a 20° angle from broadside to avoid the beam squint and specular reflection loss.

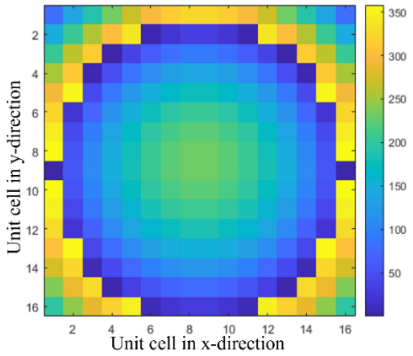

Fig. 4. Required phase distributions for the proposed RA.

The desired precise compensation phase distribution on the reflectarray aperture can be calculated as [23]:

$$\psi_{mn} = k_0 d_{mn} + \varphi_{mn} + \varphi_{\text{ref}} \quad (2)$$

Here, ψ_{mn} presents the unit cell in m-th column and the n-th row, k_0 is the wavenumber in free space, φ_{mn} is the progressive phase (pp) of the (m, n)-th unit cell in the collimated direction, and d_{mn} is the distance from the phase center of the feed to the unit cell. The additional term φ_{ref} is included to optimize the beam pattern and gain flatness during the array synthesis, and it has a range of 360°. Fig. 4 shows the distribution of the phase compensation ψ_{mn} with an optimized reference phase φ_{ref} (= -80°). Then, the height of dielectric slab h_d in each unit cell can be calculated using the following equation:

$$h_d = (360^\circ - \psi_{mn})/2\beta + 5 \text{ mm} \quad (3)$$

where β is the propagation constant of the NRD waveguide at 10 GHz, set to be 10.5 degree/mm as described before, and 5 mm is the reference height of the dielectric slab according to Fig. 4. The dielectric slabs are fabricated using a commercial fused deposition modeling (FDM) 3D printer with PLA filament, while the conductor walls are made by aluminum sheets. The slabs are then attached one by one to the surface of the conductor walls using glue to form the reflectarray, as shown in Fig. 5. The measurement of the prototype is carried out in the chamber. Since the collimated beam is expected to be at a 20° angle from the z-axis in the *yoz*-plane, the reflectarray's H-plane performance will be evaluated by rotating θ angle from -90° to 90° in the φ=90° plane, as illustrated in Fig. 6. After confirming the main beam direction of the H-plane, the E-plane performance is measured by rotating the antenna with 90°.

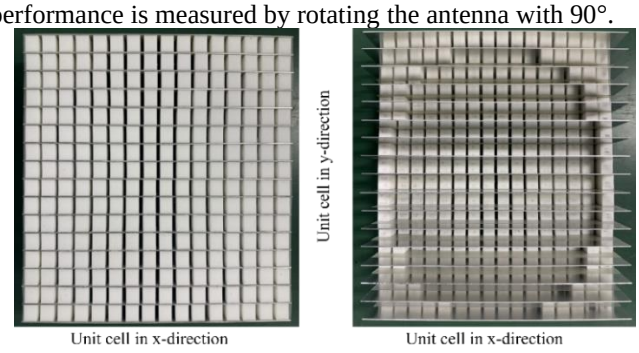

(a) (b)

Fig. 5. Photographs of the fabricated RA prototype based on NRD waveguide. (a) Top view and (b) bottom view.

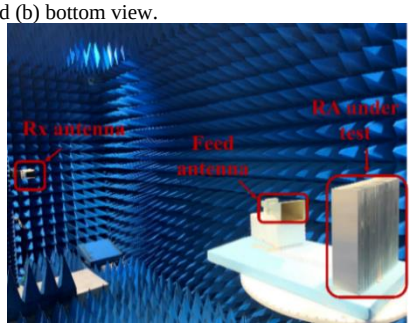

Fig. 6. Measurement setup of the proposed RA with offset feed, where Rx means receiver.

A comparison between the simulated and measured results for the RA's H-plane and E-plane patterns is performed within the operating band at the low edge, medium, and high edge frequencies, as shown in Fig. 7. Reasonable agreement between the simulation and measurement results is demonstrated. Meanwhile, as expected, the main beam appears at 20° off the broadside, while the measured sidelobe levels are lower than -15 dB in the H-plane and -17 dB in the E-plane. The cross-

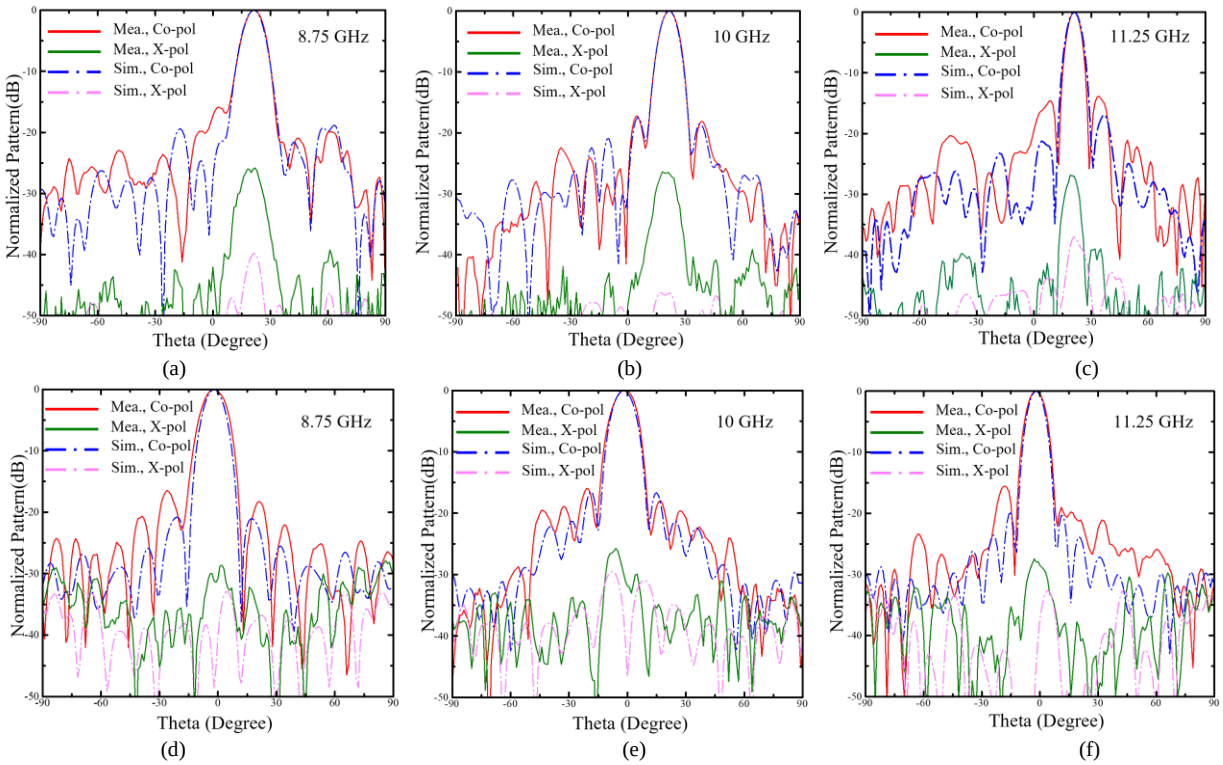

Fig. 7. Comparisons of measured and simulated patterns. H-plane at (a) 8.75, (b) 10, and (c) 11.25 GHz. E-plane at (a) 8.75, (b) 10, and (c) 11.25 GHz.

polarization (X-pol) levels are also found to be lower than -27 dB for both of the E-plane and H-plane.

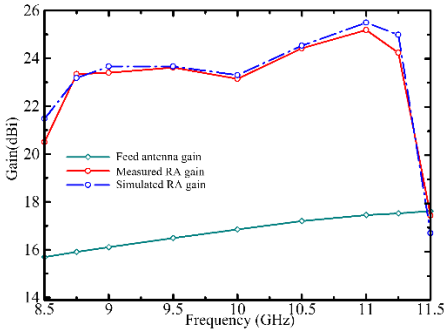

Fig. 8. Comparison of measured and simulated gain of the proposed RA with the feed antenna gain.

TABLE I
COMPARISONS OF THE PROPOSED WIDEBAND REFLECTARRAY WITH OTHER DIELECTRIC REFLECTARRAYS

Ref	No of Layers	Measured Gain BW (%)	AE (%)	Unit cell periodicity *	Thickness	Structure type
[11]	1	20.7 (1.0-dB)	14	0.5λ×0.5λ	0.77λ	Grooved FZP
[12]	1	20.9 (1.0-dB)	10	0.51λ×0.51λ	1.25λ	Grooved FZP
[13]	1	6 (1.0-dB)	38	0.99λ×0.99λ	0.37λ	Perforated plate
[14]	1	10 (1.0-dB)	31	0.55λ×0.55λ	0.69λ	DRA RA
[15]	1	7 (1.0-dB)	12.6	0.58λ×0.58λ	0.15λ	DRA RA
[16]	2	18.1 (1.0-dB)	45.6	0.45λ×0.45λ	0.55λ	Perforated plate
[17]	5	NA	43	0.63λ×0.63λ	1.38λ	Stacked layers
This work	1	18(1.0-dB) 25(2.0-dB)	45	0.43λ×0.44λ	1.0 λ	NRD waveguide

* λ means the free-space wavelength at the corresponding center frequency of each RA.

The gain of the reflectarray antenna was simulated and measured, and the results are presented in Fig. 8. The measurement exhibits a gain variation of no more than 2.0 dB over a frequency range from 8.75 GHz to 11.25 GHz, corresponding to a bandwidth of 25% centered at 10 GHz, and the peak aperture efficiency is 45%. Table I gives the performance comparisons of the proposed RA with other low-cost RAs based on 3D printing technology. In general, the proposed RA based on NRD waveguide has achieved stable and satisfactory performance over a wide bandwidth, indicating the effectiveness of the proposed design.

IV. CONCLUSION

The proposed NRD waveguide structure has been shown to be an effective unit cell for designing RAs with wideband and high efficiency performance by simulation and measurement. The phase of the reflected wave is tuned by adjusting the propagation length of the EM wave in the dielectric slab, without using any resonant element. The wideband performance has been achieved. The open air is used to reflect the EM wave without metal loss. Additionally, the NRD waveguide itself has been verified to an efficient way for minimizing metal loss as a transmission line [24]. Therefore, the proposed design will be very attractive for the millimeter-wave applications where metal loss is a significant problem. It is worth further noting that, the bandwidth can be extended if high permittivity dielectric slab is deployed with same dimension as described in Section II, which will allow for greater flexibility in the design of wideband RA.

REFERENCES

[1] T. Otsuji, K. Iwatsuki, H. Yamada and M. Yashima, "Concept of resilient electric power and information communication technology (R-EICT) converged network systems based on overall optimization of autonomous decentralized cooperative control of DC microgrids," *2021 IEEE Power & Energy Society Innovative Smart Grid Technologies Conference (ISGT)*, 2021, pp. 1-5.

[2] T. Tanaka, H. Minami, et al. "Energy-distribution platform technologies toward zero environmental impact" NTT Technical Review, vol. 19, no. 6, June 2021.

[3] X. Cao, Q. Chen, T. Tanaka, M. Kozai and H. Minami, "A 1-bit Time-Modulated Reflectarray for Reconfigurable-Intelligent-Surface Applications," *IEEE Trans. Antennas Propag.*, vol. 71, no. 3, pp. 2396-2408, March 2023.

[4] W. Wu, K.-D. Xu, Q. Chen, T. Tanaka, M. Kozai and H. Minami, "A Wideband Reflectarray Based on Single-Layer Magneto-Electric Dipole Elements With 1-bit Switching Mode," *IEEE Trans. Antennas Propag.*, vol. 70, no. 12, pp. 12346-12351, 2022.

[5] H. Luyen, Z. Yang, M. Gao, J. H. Booske and N. Behdad, "A Wideband, Single-Layer Reflectarray Exploiting a Polarization Rotating Unit Cell," *IEEE Trans. Antennas Propag.*, vol. 67, no. 2, pp. 872-883, Feb. 2019.

[6] L. Wen, S. Gao, Q. Luo, W. Hu, B. Sanz-Izquierdo and X. -X. Yang, "Wideband Circularly Polarized Reflectarray Antenna Using Rotational Symmetrical Crossed Dipoles," *IEEE Trans. Antennas Propag.*, vol. 71, no. 5, pp. 4576-4581, May 2023,

[7] Q. -Y. Guo and H. Wong, "Wideband and High-Gain Fabry–Pérot Cavity Antenna With Switched Beams for Millimeter-Wave Applications," *IEEE Trans. Antennas Propag.*, vol. 67, no. 7, pp. 4339-4347, July 2019,

[8] F. Wu, J. Wang, Y. Zhang, W. Hong and K.-M. Luk, "A broadband circularly polarized reflectarray with magneto-electric dipole elements", *IEEE Trans. Antennas Propag.*, vol. 69, no. 10, pp. 7005-7010, Oct. 2021.

[9] B. J. Xiang, X. Dai and K. -M. Luk, "A Wideband Low-Cost Reconfigurable Reflectarray Antenna With 1-Bit Resolution," *IEEE Trans. Antennas Propag.*, vol. 70, no. 9, pp. 7439-7447, Sept. 2022,

[10] R. Flamini *et al*., "Toward a Heterogeneous Smart Electromagnetic Environment for Millimeter-Wave Communications: An Industrial Viewpoint," *IEEE Trans. Antennas Propag.*, vol. 70, no. 10, pp. 8898-8910, Oct. 2022.

[11] P. Nayeri *et al*., "3D Printed Dielectric Reflectarrays: Low-Cost High-Gain Antennas at Sub-Millimeter Waves," *IEEE Trans. Antennas Propag.*, vol. 62, no. 4, pp. 2000-2008, April 2014,

[12] M. D.Wu, B. Li,Y. Zhou, D. L. Guo,Y. Liu, F.Wei, and X. Lv, "Design and measurement of a 220 GHz wideband 3-D printed dielectric reflectarray," *IEEE Antennas Wireless Propag. Lett.*, vol. 17, no. 11, pp. 20942098, Nov. 2018.

[13] M. Abd-Elhady, W. Hong, and Y. Zhang, "A Ka-band reflectarray implemented with a single-layer perforated dielectric substrate," *IEEE Antennas Wireless Propag. Lett.*, vol. 11, pp. 600603, 2012.

[14] S. Zhang, "Three-dimensional printed millimetre wave dielectric resonator reflectarray," *IET Microw., Antennas Propag.*, vol. 11, no. 14, pp. 20052009, 2017.

[15] Y.-X. Sun and K. W. Leung, "Millimeter-wave substrate-based dielectric reflectarray," *IEEE Antennas Wireless Propag. Lett.*, vol. 17, no. 12, pp. 23292333, Dec. 2018.

[16] Y. He, Z. Gao, D. Jia, W. Zhang, B. Du, and Z. N. Chen, "Dielectric metamaterial-based impedance-matched elements for broadband reflectarray," *IEEE Trans. Antennas Propag.*, vol. 65, no. 12, pp. 70197028, Dec. 2017.

[17] J. Zhu, Y. Yang, D. Mcgloin, S. Liao and Q. Xue, "3-D Printed All-Dielectric Dual-Band Broadband Reflectarray with a Large Frequency Ratio," *IEEE Trans. Antennas Propag.*, vol. 69, no. 10, pp. 7035-7040, Oct. 2021.

[18] T. Yoneyama and S. Nishida, "Non-Radiative dielectric waveguide for millimeter-wave integrated circuits," *IEEE Trans. Microwave Theory Tech.*, vol. MTT-29, pp. 1188–1192, Nov. 1981

[19] J. Malherbe, "The design of a slot array in nonradiating dielectric waveguide, part I: Theory," *IEEE Trans. Antennas Propag.*, vol. 32, no. 12, pp. 1335-1340, Dec. 1984.

[20] D. Berry, R. Malech and W. Kennedy, "The reflectarray antenna," in *IEEE Trans. Antennas Propag.*, vol. 11, no. 6, pp. 645-651, November 1963, doi: 10.1109/TAP.1963.1138112.

[21] G.-B. Wu, Y.-S. Zeng, K. F. Chan, B. -J. Chen, S.-W. Qu and C. H. Chan, "High-Gain Filtering Reflectarray Antenna for Millimeter-Wave Applications," in *IEEE Trans. Antennas Propag.*, vol. 68, no. 2, pp. 805-812, Feb. 2020

[22] Y. Liu, Y. J. Cheng, M. -H. Zhao and Y. Fan, "Dual-Band Shared-Aperture High-Efficiency Reflectarray Antenna Based on Structure-Reuse Technique," *IEEE Antennas Wireless Propag. Lett.*, vol. 20, no. 3, pp. 366-370, March 2021,

[23] J. Huang and J. A. Encinar, *Reflectarray Antennas*. Hoboken-Piscataway, NJ, USA: Wiley—IEEE Press, 2007.

[24] J. Dallaire and K. Wu, "Complete characterization of transmission losses in generalized nonradiative dielectric (NRD) waveguide," *IEEE Trans. Microwave Theory Tech.*, vol. 48, no. 1, pp. 121-125, Jan. 2000.